

Activating Distributed Visual Region within LLMs for Efficient and Effective Vision-Language Training and Inference

Anonymous ACL submission

Abstract

Large Vision-Language Models (LVLMs) typically learn visual capacity through visual instruction tuning, involving updates to both a projector and their LLM backbones. Drawing inspiration from the concept of visual region in the human brain, we investigate the existence of an analogous *visual region* within LLMs that functions as a cognitive core, and explore the possibility of efficient training of LVLMs via selective layers tuning. We use Bunny-Llama-3-8B-V for detailed experiments and LLaVA-1.5-7B and LLaVA-1.5-13B for validation across a range of visual and textual tasks. Our findings reveal that selectively updating 25% of LLMs layers, when sparsely and uniformly distributed, can preserve nearly 99% of visual performance while maintaining or enhancing textual task results, and also effectively reducing training time. Based on this targeted training approach, we further propose a novel visual region-based pruning paradigm, removing non-critical layers outside the visual region, which can achieve minimal performance loss. This study offers an effective and efficient strategy for LVLM training and inference by activating a layer-wise visual region within LLMs, which is consistently effective across different models and parameter scales.

1 Introduction

Large Vision-Language Models (LVLMs) (Li et al., 2023; Zhu et al., 2023; Bai et al., 2023; Liu et al., 2024) have emerged as an increasing research interest for interpreting and interacting with the world through both visual and linguistic channels. Existing LVLMs generally utilize advanced Large Language Models (LLMs), like FlanT5 (Chung et al., 2022) and Vicuna (Chiang et al., 2023), as their cognitive core, and align visual features from visual encoders with LLMs’ knowledge and reasoning abilities. This alignment has demonstrated remarkable performance across diverse visual tasks (Lu et al., 2022; Liu et al., 2023b; Fu et al., 2024).

LVLMs are primarily trained through visual instruction tuning (Liu et al., 2023a), which involves training both a projector and LLMs on visual instruction datasets, with optional updates to the visual encoder. Despite its efficacy, fully tuning all LLMs layers remains computationally costly, even when using efficient strategies like Low-Rank Adaptation (LoRA) (Hu et al., 2021) and its quantized variant (QLORA) (Dettmers et al., 2024). Additionally, extensive multimodal training risks degrading LLMs’ pre-trained linguistic knowledge and reasoning capabilities (Dai et al., 2024; Agrawal et al., 2024), as evidenced by LVLMs’ increased perplexity on textual tasks compared to their LLM backbone in the purple section of Fig. 1.

Inspired by specialized visual regions in the human brain (Grill-Spector and Malach, 2004) and LLMs’ brain-like versatility across tasks, we propose an analogous concept of a *visual region* within LLMs. We hypothesize that visual alignment to LLMs can only activate this specific *visual region* while preserving LLMs’ core language abilities, potentially manifesting as a layer-wise structure considering layer redundancy in LLMs (Men et al., 2024; Gromov et al., 2024). We further detailedly analyze LVLMs’ layer redundancy in Fig. 1 (green part), shows that reverting certain layers of a LVLM to its backbone LLM’ parameters minimally impacts downstream visual performance. This suggests certain layers within LLMs are non-essential for visual tasks, thereby supporting our hypothesis.

Although layer-wise freezing techniques (Zhang et al., 2024b) enable efficient LLM fine-tuning by adapting later layers for specific language tasks, they cannot be directly applied to visual tasks. Because visual alignment requires visual perception capabilities beyond textual understanding and reasoning. While Zhang et al. (2024a) propose parameter localization for visual tasks, it remains highly task-specific and data-dependent, limiting its generalizability to versatile multimodal learning and

Model Variants	Visual		Textual	
	OCRvQA	DocVQA	WikiText	Pile-10k
LLaVA	2.43	30.55	11.44	29.58
LLaVA _r (layer 0~7)	1.87	38.49 [↑]	11.37 [↑]	29.19 [↑]
LLaVA _r (layer 8~15)	1.93	32.35 [↑]	11.38 [↑]	29.21 [↑]
LLaVA _r (layer 16~23)	2.18	16.47	11.35 [↑]	29.33 [↑]
LLaVA _r (layer 24~31)	2.11	17.47	11.36 [↑]	29.27 [↑]
Vicuna (all layers)	80.75	175.10	11.32	28.38

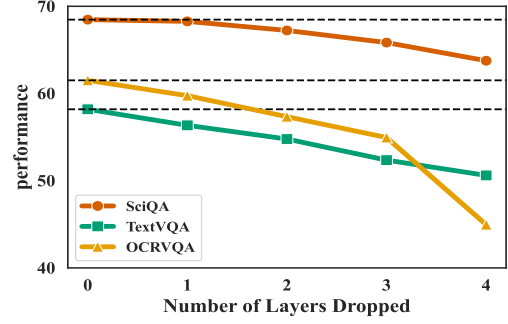


Figure 1: **Left:** Perplexity of LLaVA with selected layers (in parentheses) reverted to Vicuna parameters on visual and textual tasks. Arrows indicate perplexity increases relative to LLaVA (visual tasks) and Vicuna (textual tasks). Both results suggest layer redundancy in LVLMs and degraded linguistic capability. **Right:** Accuracy of LLaVA-1.5-7B when pruning certain layers based on angular distance scores (Gromov et al., 2024).

neglecting the preservation of linguistic capabilities. To bridge this gap, we identify a general-purpose visual region within LLMs for efficient LVLM training across diverse tasks without diminishing linguistic performance. Specifically, we aim to investigate two key questions: (1) Where is this visual region located within LLMs? (2) What is the necessary scale of layers in this visual region to ensure effective and efficient LVLMs training?

To this end, we embark on empirical experiments with Bunny-Llama-3-8B-V (He et al., 2024) across diverse visual tasks. Our findings indicate that **sparingly and uniformly distributed layers within LLMs are the optimal position for visual learning** while simultaneously preserving textual performance. This strategic visual region selection also outperforms previous layer importance strategies. Notably, **updating only 25% of layers achieves nearly 99% performance on visual tasks** while effectively saving training time. We further validate this conclusion with LLaVA-1.5-7B and LLaVA-1.5-13B (Liu et al., 2023a), demonstrating its consistent applicability across models and parameter scales. Specifically, we achieve time reductions of nearly 23% for LLaVA-1.5-7B and LLaVA-1.5-13B, and 12% for Bunny-Llama-3-8B-V.

Additionally, as shown in Figure 1 (right), we find that commonly used layer-pruning strategies are ineffective for LVLMs, with even minimal layer removal causing significant performance degradation. In response, we propose a visual region-based pruning paradigm that selectively prunes less-important layers outside the visual region after targeted training. Specifically, we follow the angular distance based layer importance strategy (Gromov et al., 2024) outside the visual region, and experimental results demonstrate that our paradigm is

effective to minimize performance decline. Overall, our work highlights promising potential for more efficient LVLMs training and inference.

2 Preliminary of LVLMs

2.1 Model Architecture

Mainstream LVLMs consist of three components: a LLM, a visual encoder, and a projector or connection module, aim to effectively leverage the capabilities of both the pre-trained visual model and LLMs. The visual encoder extracts visual features from images, commonly utilizing pre-trained models such as CLIP ViT-L/14 (Radford et al., 2021). The connection module then projects these extracted features into word embedding space understandable by LLMs, commonly employing techniques such as linear projection (Tsimpoukelli et al., 2021), Q-former (Li et al., 2023), or cross-attention layers (Alayrac et al., 2022). This enables LVLMs based on LLMs cores, like Vicuna (Chiang et al., 2023), FlanT5 (Chung et al., 2022), and LLaMA (Touvron et al., 2023) to process visual information in a similar manner as text.

2.2 Model Training

The training process of LVLMs can be broadly divided into two phases: pre-training and supervised fine-tuning. Unlike LLMs, both the pre-training and supervised fine-tuning of LVLMs utilize supervised image-text pairs for visual instruction tuning. The pre-training stage primarily utilizes large-scale captioning instruction data, which requests the model to briefly describe images. This phase enables the model to interpret image content, usually with LLMs' weights frozen and the visual encoder optionally updated. Some works such as

Qwen-VL (Bai et al., 2023), also expand the pre-training to incorporate additional tasks like visual question answering, and update the LLMs component accordingly. During the supervised fine-tuning stage, high-quality instruction data are employed to enhance the LVLMs’ ability in following diverse visual instructions and engaging in conversations. The visual encoder in this stage is typically kept static while the LLMs are tuned. During both stages, the projector is consistently updated, ensuring the model’s evolving ability to bridge visual and textual data.

3 Experimental Setup

In this study, we conduct empirical experiments on Bunny-Llama-3-8B-V to investigate our hypothesis regarding the existence of a specific *visual region* within LLMs (Sec. 4.1~4.3), and apply our findings on LLaVA-1.5-7B and LLaVA-1.5-13B to validate its general applicability across different model configurations (Sec. 5.1).

3.1 LVLM Implementation

We employ Bunny-Llama-3-8B-V for investigation experiments, which builds upon the 32-layer Llama3-8B (Touvron et al., 2023), and LLaVA-1.5-7B/13B, built on the 32/40-layer Vicuna-1.5-7B/13B (Chiang et al., 2023), for validation. Since the LLM components remain frozen during pre-training, our focus is on the supervised fine-tuning stage using 695K and 665K language-image instruction-following instances for Bunny and LLaVA, respectively. Considering computational constraints, we use the LoRA (Hu et al., 2021) strategy, highlighting that our approach is complementary to other efficient training methods. Training was conducted with DeepSpeed (Song et al., 2023) configured for zero3 optimization on 8xA800 GPUs. Additional implementation details are available in the Appendix.

3.2 Evaluation Tasks

Our investigation spans diverse visual perception and cognition tasks, to comprehensively evaluate models and thoroughly examine our hypothesis.

3.2.1 Visual perception tasks

Visual perception tasks assess models’ ability to interpret and understand surface-level visual features, such as object identification and scene recognition, mirroring human sensory perception process.

- OCRVQA (Mishra et al., 2019): VQA by reading text in images through optical character recognition (OCR). We adopt the accuracy calculation method from (Bai et al., 2023) on the test set, allowing a certain margin of error.
- DocVQA (Mathew et al., 2021): VQA by interpreting document images. For DocVQA’s validation set, we employ the same evaluation method and metric as in OCRVQA.
- RefCOCOg (Yu et al., 2016): A variant of RefCOCO (Kazemzadeh et al., 2014) featuring more complex object referring expressions in COCO images (Lin et al., 2014). We assess the reference expression generation task on the test set using Intersection over Union as the metric.
- TDIUC (Kafle and Kanan, 2017): a VQA task suite across 12 categories, primarily perception tasks (e.g., object presence, counting, recognition) with some cognition tasks (e.g., positional reasoning, affordance, subordinate). Accuracy is measured on the validation set.

3.2.2 Visual cognition tasks

Contrary to perception tasks, cognition tasks require deeper reasoning based on visual stimuli, drawing on prior knowledge and advanced decision-making abilities learned within LLMs. This process resembles cognitive thinking and manipulation in human mental activities.

- MMBench (Liu et al., 2023b): a benchmark mainly for cognition tasks, with some fine-grained perception tasks requiring knowledge and reasoning. For simpler model variant comparison, we calculate accuracy on the dev subset instead of submitting to the evaluation server.
- GQA (Hudson and Manning, 2019): a dataset featuring real-world visual reasoning and compositional question answering.
- ScienceQA (Lu et al., 2022): sourced from elementary and high school science curricula, requiring external knowledge and reasoning. We focus on questions with image context.
- TextVQA (Singh et al., 2019): a dataset requiring reasoning about text in images. For TextVQA, ScienceQA, and GQA, we use the LLaVA evaluation codes to measure accuracy.

4 Visual Region Investigation

We first analyze the position and scale of the layerwise-structure vision region within its LLM

Model Version	Perception				Cognition				Avg
	OCRvQA	DocVQA	RefCOCOg	TDIUC	MMBench	GQA	ScienceQA	TextVQA	
All layers	64.26%	29.45%	50.12%	83.84%	74.74%	64.29%	79.28%	62.11%	63.51%
Heuristic Selections									
Sparse & Uniform	62.65%	29.51%	48.33%	83.68%	73.88%	63.68%	78.78%	62.43%	62.88%
Consecutive Lower	61.38%	22.47%	46.49%	83.27%	73.63%	62.33%	75.26%	62.26%	60.89%
Consecutive Lower-middle	62.54%	26.13%	48.17%	83.77%	72.51%	62.81%	77.14%	60.96%	61.75%
Consecutive Upper-middle	62.32%	28.06%	43.12%	83.40%	70.27%	61.28%	78.83%	59.33%	60.83%
Consecutive Top	60.48%	26.47%	39.92%	83.22%	67.96%	60.30%	77.54%	58.71%	58.08%
Hybrid Top-Lower	57.63%	29.76%	41.79%	83.26%	72.25%	62.71%	77.99%	62.74%	61.02%
Importance-based Selections									
Image Attention Score	63.65%	24.53%	43.62%	83.90%	72.59%	62.82%	77.59%	61.99%	61.34%
Parameter Change Ratio	63.94%	26.94%	47.67%	83.88%	73.54%	63.21%	78.68%	61.73%	62.45%
Block Influence Score	62.38%	28.45%	46.37%	83.73%	71.13%	61.93%	77.34%	59.93%	61.41%
Multimodal BI Score	61.48%	28.80%	46.68%	83.74%	73.02%	63.23%	77.24%	62.23%	62.05%
Angular Distance	60.95%	27.71%	46.74%	83.49%	73.88%	62.11%	77.14%	62.76%	61.85%

Table 1: Performance comparison of Bunny-LLaMA-3-8B-V tuned with *different layer selection methods (8 layers)*. Bold numbers indicate the best performance in each column (excluding “all layers”).

core on Bunny-Llama-3-8B-V, to answer the following two questions.

4.1 Where are visual region layers located within LLMs for effective visual learning?

To demonstrate the optimal positioning of the visual region in LLMs for effective and efficient visual learning, we re-train Bunny-Llama-3-8B-V by updating 25% of layers (8 layers)¹ under various selection configurations. As pre-training does not involve LLM optimization, we focus on supervised fine-tuning, starting from the pre-trained checkpoint. We specifically explore different positional selection strategies as detailed below.

- **Heuristic Layer Selection** (1) We intuitively hypothesize that tuning *sparsely and uniformly distributed layers* (0,4,8,12,18,22,26,30) preserves LLMs’ existing knowledge and reasoning abilities while enabling visual learning. (2) We experiment with tuning *consecutive 8-layer blocks* at different positions in LLMs: lower layers (0~7), lower-middle layers (8~15), upper-middle layers (16~23), and top layers (24~31), with the latter being a common practice of efficient downstream fine-tuning (Liao et al., 2024). (3) We test a hybrid of lower and top layers (0~3, 28~31).
- **Importance-based Layer Selection** We compare layer selection strategies based on varying importance metrics. (1) *Image Attention Score*: We compute the average attention score

on all image tokens at each layer to gauge the layer’s affinity for image information. The top 8 layers with the highest scores are selected (1,2,3,4,5,27,29,31). (2) *Parameter Change Ratio* (Zhao et al., 2023): 8 layers with the highest relative parameter change ratios (averaged all parameters in each layer) in Bunny-Llama-3-8B-V compared to its backbone Llama are selected (0,2,9,12,23,24,25,26). (3) *Block Influence (BI) Score* (Men et al., 2024): Using Flickr30k dataset, we calculate hidden state transformations at each layer as the BI score, and select 8 layers with the highest scores (12,15,18,25,27,29,30,31). (4) *Multimodal BI Score*: We propose a multimodal variant that average hidden state transformations respectively of visual tokens and textual tokens, and select 8 layers with highest scores (0,1,2,3,4,5,9,31). (5) *Angular Distance Score* (Gromov et al., 2024): The top 8 layers with the highest angular distances between consecutive layer inputs are selected (0,1,2,3,5,6,7,8). Detailed calculations for these metrics are provided in Appendix A.

The results are shown in Table 1. We observe that tuning sparsely and uniformly distributed layers achieves the best overall performance across perception and cognition tasks, closely matching the all-layers upper bound. In contrast, consecutive layers generally underperform, likely due to limited diversity in similar representations across adjacent layers (Kornblith et al., 2019), which hinders adaptability to various tasks. This further under-

¹We use the 8-layer configuration as a testbed for its balance of efficiency and effectiveness.

Model Scale	Perception				Cognition				Avg
	OCRVQA	DocVQA	RefCOCOg	TDIUC	MMBench	GQA	ScienceQA	TextVQA	
32 layers	64.26%	29.45%	50.12%	83.84%	74.74%	64.29%	79.28%	62.11%	63.51%
16 layers	62.42%	26.43%	49.15%	84.04%	74.83%	64.10%	78.93%	62.96%	62.86% (98.98%)
8 layers	62.65%	29.51%	48.33%	83.68%	73.88%	63.68%	78.78%	62.43%	62.88% (99.00%)
6 layers	62.25%	29.76%	47.71%	84.01%	75.00%	62.93%	77.54%	62.92%	62.78% (98.85%)
4 layers	62.40%	28.89%	46.00%	83.99%	73.71%	62.66%	77.69%	62.74%	62.26% (98.03%)
2 layers	57.96%	28.49%	44.67%	83.15%	72.68%	61.00%	78.48%	60.35%	60.85% (95.81%)
1 layer	53.68%	24.33%	38.47%	82.92%	68.64%	59.19%	77.69%	58.32%	57.91% (91.18%)

Table 2: Performance comparison of Bunny-Llama-3-8B-V fine-tuned with *different numbers of layers*. Bold numbers represent the best performance in each column. Values in parentheses denotes the percentage relative to the performance achieved by tuning all layers.

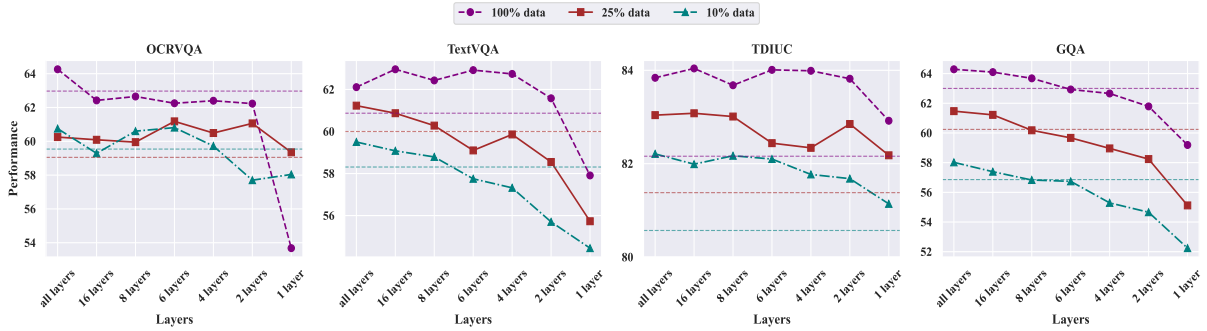


Figure 2: Performance variation of the re-trained Bunny-Llama-3-8B-V model across *different training data scales* during the supervised fine-tuning stage, with tuning varying number of layers. Dashed lines indicate 98% of the performance achieved by tuning all layers with the corresponding training data scale.

scores the superiority of sparsely and uniformly distributed layers. Notably, tuning top layers yields the worst performance, deviating from the conventional practice in domain-specific fine-tuning, where the last few layers are typically adjusted for downstream tasks (Liao et al., 2024). This highlights a significant distinction between adapting to new modalities and new downstream domains. Furthermore, while importance-based metrics are effective for layer pruning during LLMs inference, they are less effective than our empirically selected sparse and uniform layers for visual learning.

4.2 What is the necessary scale of layers for effective and efficient LVLMs training?

To investigate the necessary scale of this visual region to enable LVLMs to receive visual signals and align with linguistic features, we re-train Bunny-Llama-3-8B-V by updating varying number of layers. We respectively experiment with configurations of 32, 16, 8, 6, 4, 2 and 1 layers, with all selected layers uniformly distributed across all layers². This selection strategy is based on our finding

²Specifically, we select all even-numbered layers for the 16-layer configuration; layer 0, 4, 8, 12, 18, 22, 26, 30 for the

that sparsely and uniformly distributed layers are the optimal position for effective visual learning.

The results of tuning varying scales of layers on visual perception and cognition tasks are summarized in Table 2. Tuning 20~25% of the layers (6 and 8 layers) retains approximately 98% of the performance achieved by tuning all LLMs layers of Bunny-Llama-3-8B-V, with 25% (8 layers) preserving up to 99%. However, updating fewer than 4 layers leads to a significant performance drop, particularly in perception tasks that heavily relies on visual interpretation, highlighting the necessity of tuning at least 12.5% of the layers (4 layers) for effective visual alignment.

4.3 Trend between Data Size and Visual Region Scale

We further explore the trend between data size and the optimal layer count for effective visual instruction tuning. Using random subsets of 100%, 25%

8-layer setup; layer 0, 6, 12, 18, 24, 30 for the 6-layer setup; and layer 0, 10, 20, 30 for the 4-layer configuration (Our experiments show that using layer 30 or 31 leads to comparable results). For 2 layers and 1 layers that can not selected uniformly, we choose layers with highest block influence scores, i.e., layer 0 and 31 for 2 layers, and layer 31 for 1 layer.

Model Scale	Perception				Cognition				Avg
	OCRvQA	DocVQA	RefCOCOg	TDIUC	MMBench	GQA	ScienceQA	TextVQA	
LLaVA-1.5-7B									
32 layers	61.51%	19.46%	49.01%	83.40%	66.67%	62.98%	68.47%	58.19%	58.71%
16 layers	64.01%	20.75%	48.02%	83.47%	64.00%	62.43%	67.53%	58.27%	58.56% (99.74%)
8 layers	62.19%	21.10%	47.71%	83.10%	63.92%	61.60%	68.17%	57.35%	58.14% (99.03%)
6 layers	61.39%	22.84%	46.54%	83.31%	61.77%	61.08%	68.32%	56.19%	57.69% (98.26%)
4 layers	63.28%	21.01%	43.47%	83.14%	60.82%	60.48%	67.97%	54.48%	56.83% (96.80%)
2 layers	54.54%	19.10%	41.90%	81.47%	57.22%	57.38%	65.84%	53.27%	53.84% (91.70%)
1 layer	53.16%	16.96%	33.29%	81.20%	51.89%	55.83%	64.50%	45.51%	50.29% (85.66%)
LLaVA-1.5-13B									
40 layers	67.60%	25.19%	50.26%	83.61%	68.38%	63.29%	71.64%	60.21%	61.27%
10 layers	65.17%	23.56%	48.27%	83.57%	66.58%	62.01%	70.75%	59.13%	59.88% (97.73%)
9 layers	66.47%	23.65%	49.29%	83.74%	65.61%	62.31%	72.14%	59.71%	60.37% (98.53%)

Table 3: Performance Comparison of LLaVA-1.5 with different model scales tuned with different numbers of layers. Bold numbers represent the best performance in each column. Values in parentheses denotes the percentage relative to the performance achieved by tuning all layers.

and 10% from a pool of 695K visual instruction-following instances, we tune Bunny-Llama-3-8B-V with varying numbers of layers following the same selection strategy as the full dataset. We report the performance trends across four datasets, OCRVQA, TextVQA, TDIUC and GQA. As shown in Figure 2, tuning 25% of the layers consistently achieves over 98% of full performance across different data sizes while reducing training time. This approach offers a resource-efficient pathway for optimizing hyperparameters and training data selection by tuning such a visual region before finalizing the model with all layers. Moreover, even with smaller datasets, tuning fewer than 4 layers still results in notable performance declines.

5 Further Analysis

5.1 Generalizability Validation

To validate our findings of visual region beyond Bunny-Llama-3-8B-V, we take LLaVA-1.5-7B and LLaVA-1.5-13B as additional testbeds to assess the generalizability across LVLMs with different LLM backbones and parameter scales. Following the setup in Sec. 4.2, we re-train both models with different number of layers that are sparsely and uniformly distributed within their respective backbones, Vicuna-1.5-7B and Vicuna-1.5-13B. Results presented in Table 3 show that under our visual region positioning strategy, tuning approximately 25% of the layers consistently yield 98% of the full performance. This demonstrates that our approach generalizes effectively across LVLMs.

5.2 Computational Cost

To demonstrate the efficiency of visual region-based tuning, we report the computational costs associated with tuning different numbers of layers across various models using the LoRA strategy. For fair comparison across setups with different numbers of GPUs (specifically A800 GPUs in this analysis), we compute the product of the number of GPUs and running hours as a measure of computational cost. From Figure 3, Table 2 and Table 3, tuning a visual region comprising up to 25% of layers (8 layers for LLaVA-1.5-7B and Bunny-Llama3-8B-V, 10 layers for LLaVA-1.5-13B) can achieve 98% of full performance while achieving substantial reductions in computational overhead.

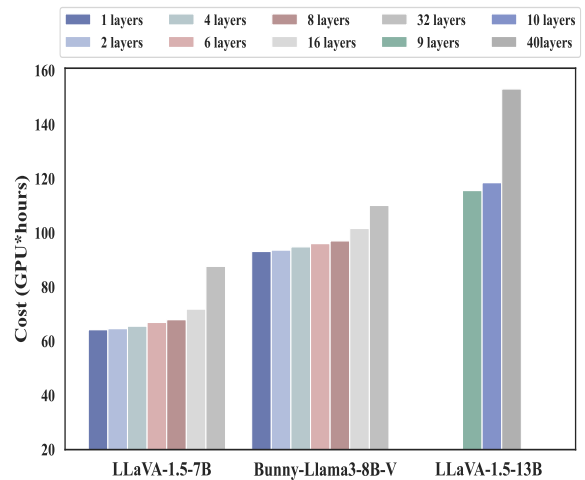


Figure 3: Computational costs for tuning LLaVA-1.5-7B, Bunny-Llama-3-8B-V, and LLaVA-1.5-13B with different number of layers using LoRA.

Specifically, we reduce training time by 23% for LLaVA models and 13% for Bunny. These results highlight that the effectiveness of visual region-based tuning in training LVLMs efficiently with minimal performance trade-offs.

5.3 Evaluation of Textual Tasks

As highlighted in (Dai et al., 2024; Agrawal et al., 2024) and illustrated in Figure 1, multimodal training risks significant degradation of LLMs’ pre-trained linguistic knowledge and reasoning capabilities. To verify whether training our sparsely and uniformly distributed visual region compromises the model linguistic capacity, we extend our experiments to two text-only question answering datasets, MMLU (Hendrycks et al., 2020) and BIG-bench-Hard (Suzgun et al., 2022), covering a wide range of topics and fields. We use “Answer with the option’s letter from the given choices directly” and “Please answer this question in a word or phrase” as the prompts for MMLU and BIG-bench-Hard. We calculate the multi-choice accuracy as the evaluation metric, allowing models to provide additional explanations alongside its responses. We adopt a five-shot prompting strategy for MMLU and a zero-shot strategy for BIG-bench-Hard.

Model Version	MMLU	BIG-bench-hard
Bunny-LLaMA3-8B-V		
Fully-trained (32 layers)	60.27%	30.93%
Partial-trained(8 layers)	63.36%	31.50%
LLM-Backbone	66.01%	57.93%
LLaVA-1.5-7B		
Fully-trained (32 layers)	50.52%	26.85%
Partial-trained (8 layers)	50.74%	31.64%
LLM-Backbone	49.78%	29.33%

Table 4: Performance on text-only tasks. The LLM backbones of Bunny-LLaMA3-8B-V and LLaVA-1.5-7B are respectively LLaMA3-8B and Vicuna-1.5-7B.

As shown in Table 4, fully-trained LVLMs generally exhibit decreased performance on text-only tasks compared to their LLM backbones, particularly on the challenging BIG-bench-Hard dataset. In contrast, our selectively trained LVLMs consistently achieve better performance than fully-trained LVLMs, even sometimes outperform their LLMs backbones. These results support our hypothesis regarding the positioning of visual region, that tuning sparsely and uniformly distributed layers better preserves LLMs’ pre-existing linguistic knowledge

and reasoning capabilities, while full training may cause minor disruptions.

6 Visual Region-Based Layer Pruning

Beyond layer selection for efficient LVLMs training, we explore whether the visual region can also benefit LVLM efficient inference. Although layer pruning techniques (Men et al., 2024; Ma et al., 2023) have been widely developed for LLM inference, they prove ineffective for LVLMs. As shown in Figure 1 (right), minimal layer removal causing significant performance degradation on visual tasks even using advanced angular distance based pruning strategy (Gromov et al., 2024).

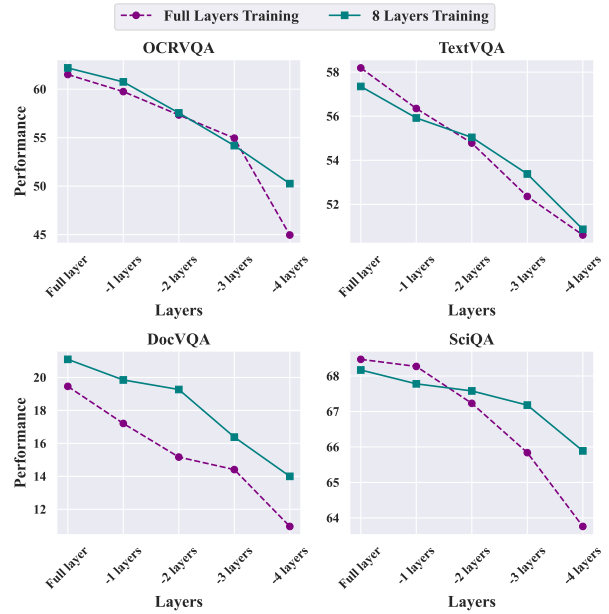


Figure 4: Results of pruning LLaVA-1.5-7B using angular distance-based strategy with 0~4 layers removed. Dashed lines represent pruning applied to the fully trained model while solid layers denote our visual region-based pruning within the targeted trained model.

Building on our visual region targeted training, we propose a visual region-based pruning paradigm that selectively prunes less-important layers outside the visual region after training. Specifically, we follow the angular distance based layer importance metric and select 0~4 layers with the lowest angular distance outside the visual region. We do not evaluate pruning beyond this range as removing additional layers in LVLMs would lead to significant performance collapse. We evaluate this approach on LLaVA-1.5-7B across four datasets: OCRVQA, TextVQA, DocVQA and SciQA. As shown in Figure 4, our paradigm generally maintain higher performance, especially when pruning

3~4 layers, even though the visual region targeted trained model performs slightly worse than fully trained model without pruning. This result demonstrates that our paradigm effectively minimizes performance degradation compared to pruning in full-layer trained LVLMs.

7 Related Work

7.1 Efficient Training and Inference

Recent research community has witnessed an emergent interest in LLMs (Touvron et al., 2023; Chiang et al., 2023) and LVLMs (Li et al., 2023; Zhu et al., 2023; Bai et al., 2023; Liu et al., 2024) due to their remarkable ability to interpret and interact with the world via linguistic and visual channels. With the sustainably increased scale of LLMs and LVLMs, training or inference using all model parameters are cost for practical deployment. There are numerous techniques for efficient model training and inference. For instance, quantization reduce the memory footprint of models by decreasing the precision of model weights (Dettmers et al.; Dettmers and Zettlemoyer, 2023; Xiao et al., 2023). Low rank adapters enable cost-effective fine-tuning by updating only a small subset of the adapter parameters (Hu et al., 2021; Karimi Mahabadi et al., 2021).

Moreover, LLMs exhibit significant redundancy at the layer level, making training or inference with all layers computationally wasteful, and this redundancy is established for LVLMs as well, where LLMs serve as the core cognitive brain for visual learning. In responding, layer-wise freezing techniques (Zhang et al., 2024b; Liang et al., 2023; Pan et al., 2024) and layer pruning strategies (Men et al., 2024; Ma et al., 2023; Gromov et al., 2024) are proposed to enable efficient LLM fine-tuning and inference. However, they are designed for LLMs and fail to generalize effectively to visual learning, often resulting in substantial performance degradation. While Zhang et al. (2024a) introduce parameter localization for visual tasks, their approach is highly task-specific and data-dependent, limiting its applicability to versatile visual learning and neglecting the preservation of linguistic capabilities. In contrast, we propose a more efficient layer-selected strategy for LVLMs training and inference.

7.2 Functional Regions in LLMs

The existing literature on cognitive science and brain localization indicates that different regions

among the human brain are dedicated to specific functions (Fedorenko and Varley, 2016), such as frontotemporal language processing region localized by Scott et al. (2017). Grill-Spector and Malach (2004) highlight the existence of visual regions in neuroscience (Grill-Spector and Malach, 2004). These insights have inspired an analogy with LLMs, increasingly viewed as cognitive core for remarkable performance across diverse tasks, mirroring the human brain’s functionality in terms of overall planning and processing. For example, Aw et al. (2023) propose that LLMs can be aligned to the human brain through instruction-tuning. Building upon this parallel, Zhao et al. (2023) unveil a core linguistic region within LLMs, accounting approximately 1% of the model’s parameters. Li and Li (2024) identify a duality between Tulving’s synergistic ecphory model (SEM) of memory and LLMs’ emergent abilities. Drawing inspiration from these, our research focuses on defining a vision region within LLMs, suggesting a more effective and efficient pipeline to optimizing LVLMs for visual tasks.

8 Conclusion

In this study, we introduce an effective and efficient training paradigm for LVLMs by activating a specific *visual region* within LLMs. This offers a new pipeline for advancing LVLMs which first identify such *visual region* using limited data followed by efficient continual training. Specifically, we investigating the necessity of tuning all layers within LLM cores, and propose the concept of a specialized *visual region* within LLMs. We conduct extensive empirical experiments with Bunny-LLaMA-3-8B-V, covering a range of visual and textual tasks. Our results reveal that selectively updating no more than 25% of sparsely and uniformly layers, can preserve nearly 99% visual performance, while also yielding comparable results in textual tasks. This targeted LVLMs’ training approach is consistently effective for different models and parameter scales, effectively reducing training time by 23% for LLaVA models and 12% for Bunny-LLaMA-3-8B-V. Additionally, we propose a visual region-based layer pruning by strategy removing non-critical layers outside the visual region and achieve minimal performance drop. Overall, our work presents a promising pathway for more efficient LVLMs training and inference, while complementing existing efficient training methods.

Limitations

Experimented Models Our work primarily focuses on LLaVA-1.5 family and Bunny-LLama3-8B-V to demonstrate the effectiveness and efficiency of our proposed training and inference paradigms for LVLMS. Future work will expand to a broader range of models to further validate the generalizability of our approach. Additionally, we will explore extensions to other modalities such as speech, and investigate the existence of other modality-specific regions to develop more versatile and scalable multimodal models.

Sparse Architectures While our approach effectively reduces training and inference costs by activating the *visual region*, it currently operate in a layer-wise dense manner. Future efforts will focus on integrating our method with sparse model architectures to optimize *visual region* activation. For example, explore routing mechanisms targeting modality-specific partitions within models to implement sparse mixture-of-expert architectures with specialized functional areas, analogous to the functional regions of the human brain.

References

- Pravesh Agrawal, Szymon Antoniak, Emma Bou Hanna, Devendra Chaplot, Jessica Chudnovsky, Saurabh Garg, Theophile Gervet, Soham Ghosh, Amélie Héliou, Paul Jacob, et al. 2024. Pixtral 12b. *arXiv preprint arXiv:2410.07073*.
- Jean-Baptiste Alayrac, Jeff Donahue, Pauline Luc, Antoine Miech, Iain Barr, Yana Hasson, Karel Lenc, Arthur Mensch, Katherine Millican, Malcolm Reynolds, et al. 2022. Flamingo: a visual language model for few-shot learning. *Advances in Neural Information Processing Systems*, 35:23716–23736.
- Khai Loong Aw, Syrielle Montariol, Badr AlKhamissi, Martin Schrimpf, and Antoine Bosselut. 2023. Instruction-tuning aligns llms to the human brain. *arXiv preprint arXiv:2312.00575*.
- Jinze Bai, Shuai Bai, Shusheng Yang, Shijie Wang, Sinan Tan, Peng Wang, Junyang Lin, Chang Zhou, and Jingren Zhou. 2023. Qwen-vl: A frontier large vision-language model with versatile abilities. *arXiv preprint arXiv:2308.12966*.
- Wei-Lin Chiang, Zhuohan Li, Zi Lin, Ying Sheng, Zhanghao Wu, Hao Zhang, Lianmin Zheng, Siyuan Zhuang, Yonghao Zhuang, Joseph E. Gonzalez, Ion Stoica, and Eric P. Xing. 2023. *Vicuna: An open-source chatbot impressing gpt-4 with 90%* chatgpt quality*.

- Hyung Won Chung, Le Hou, Shayne Longpre, Barret Zoph, Yi Tay, William Fedus, Yunxuan Li, Xuezhi Wang, Mostafa Dehghani, Siddhartha Brahma, et al. 2022. Scaling instruction-finetuned language models. *arXiv preprint arXiv:2210.11416*.
- Wenliang Dai, Nayeon Lee, Boxin Wang, Zhuolin Yang, Zihan Liu, Jon Barker, Tuomas Rintamaki, Mohammad Shoeybi, Bryan Catanzaro, and Wei Ping. 2024. Nvlm: Open frontier-class multimodal llms. *arXiv preprint arXiv:2409.11402*.
- Tim Dettmers, Mike Lewis, Younes Belkada, and Luke Zettlemoyer. Llm.int8(): 8-bit matrix multiplication for transformers at scale, 2022. *CoRR abs/2208.07339*.
- Tim Dettmers, Artidoro Pagnoni, Ari Holtzman, and Luke Zettlemoyer. 2024. Qlora: Efficient finetuning of quantized llms. *Advances in Neural Information Processing Systems*, 36.
- Tim Dettmers and Luke Zettlemoyer. 2023. The case for 4-bit precision: k-bit inference scaling laws. In *International Conference on Machine Learning*, pages 7750–7774. PMLR.
- Evelina Fedorenko and Rosemary Varley. 2016. Language and thought are not the same thing: evidence from neuroimaging and neurological patients. *Annals of the New York Academy of Sciences*, 1369(1):132–153.
- Chaoyou Fu, Peixian Chen, Yunhang Shen, Yulei Qin, Mengdan Zhang, Xu Lin, Jinrui Yang, Xiwu Zheng, Ke Li, Xing Sun, Yunsheng Wu, and Rongrong Ji. 2024. *Mme: A comprehensive evaluation benchmark for multimodal large language models*. *Preprint, arXiv:2306.13394*.
- Kalanit Grill-Spector and Rafael Malach. 2004. The human visual cortex. *Annu. Rev. Neurosci.*, 27:649–677.
- Andrey Gromov, Kushal Tirumala, Hassan Shapourian, Paolo Glorioso, and Daniel A Roberts. 2024. The unreasonable ineffectiveness of the deeper layers. *arXiv preprint arXiv:2403.17887*.
- Muyang He, Yexin Liu, Boya Wu, Jianhao Yuan, Yueze Wang, Tiejun Huang, and Bo Zhao. 2024. Efficient multimodal learning from data-centric perspective. *arXiv preprint arXiv:2402.11530*.
- Dan Hendrycks, Collin Burns, Steven Basart, Andy Zou, Mantas Mazeika, Dawn Song, and Jacob Steinhardt. 2020. Measuring massive multitask language understanding. *arXiv preprint arXiv:2009.03300*.
- Edward J Hu, Yelong Shen, Phillip Wallis, Zeyuan Allen-Zhu, Yanzhi Li, Shean Wang, Lu Wang, and Weizhu Chen. 2021. Lora: Low-rank adaptation of large language models. *arXiv preprint arXiv:2106.09685*.

662	Drew A Hudson and Christopher D Manning. 2019.	Haotian Liu, Chunyuan Li, Qingyang Wu, and Yong Jae	716
663	Gqa: A new dataset for real-world visual reasoning	Lee. 2024. Visual instruction tuning. <i>Advances in</i>	717
664	and compositional question answering. In <i>Proceed-</i>	<i>neural information processing systems</i> , 36.	718
665	<i>ings of the IEEE/CVF conference on computer vision</i>		
666	<i>and pattern recognition</i> , pages 6700–6709.		
667	Xu Jia, Efstratios Gavves, Basura Fernando, and	Yuan Liu, Haodong Duan, Yuanhan Zhang, Bo Li,	719
668	Tinne Tuytelaars. 2015. Guiding long-short term	Songyang Zhang, Wangbo Zhao, Yike Yuan, Jiaqi	720
669	memory for image caption generation . <i>Preprint</i> ,	Wang, Conghui He, Ziwei Liu, et al. 2023b. Mm-	721
670	arXiv:1509.04942.	bench: Is your multi-modal model an all-around	722
671	Kushal Kafle and Christopher Kanan. 2017. An analy-	player? <i>arXiv preprint arXiv:2307.06281</i> .	723
672	sis of visual question answering algorithms. In <i>Pro-</i>		
673	<i>ceedings of the IEEE international conference on</i>	Pan Lu, Swaroop Mishra, Tanglin Xia, Liang Qiu, Kai-	724
674	<i>computer vision</i> , pages 1965–1973.	Wei Chang, Song-Chun Zhu, Oyvind Taffjord, Peter	725
675	Rabeeh Karimi Mahabadi, James Henderson, and Se-	Clark, and Ashwin Kalyan. 2022. Learn to explain:	726
676	bastian Ruder. 2021. Compacter: Efficient low-rank	Multimodal reasoning via thought chains for science	727
677	hypercomplex adapter layers. <i>Advances in Neural</i>	question answering. <i>Advances in Neural Information</i>	728
678	<i>Information Processing Systems</i> , 34:1022–1035.	<i>Processing Systems</i> , 35:2507–2521.	729
679	Sahar Kazemzadeh, Vicente Ordonez, Mark Matten,	Xinyin Ma, Gongfan Fang, and Xinchao Wang. 2023.	730
680	and Tamara Berg. 2014. Referitgame: Referring to	Llm-pruner: On the structural pruning of large lan-	731
681	objects in photographs of natural scenes. In <i>Proceed-</i>	guage models. <i>Advances in neural information pro-</i>	732
682	<i>ings of the 2014 conference on empirical methods in</i>	<i>cessing systems</i> , 36:21702–21720.	733
683	<i>natural language processing (EMNLP)</i> , pages 787–	Minesh Mathew, Dimosthenis Karatzas, and C. V. Jawa-	734
684	798.	har. 2021. Docvqa: A dataset for vqa on document	735
685	Simon Kornblith, Mohammad Norouzi, Honglak Lee,	images . <i>Preprint</i> , arXiv:2007.00398.	736
686	and Geoffrey Hinton. 2019. Similarity of neural	Xin Men, Mingyu Xu, Qingyu Zhang, Bingning Wang,	737
687	network representations revisited. In <i>International</i>	Hongyu Lin, Yaojie Lu, Xianpei Han, and Weipeng	738
688	<i>conference on machine learning</i> , pages 3519–3529.	Chen. 2024. Shortgpt: Layers in large language	739
689	PMLR.	models are more redundant than you expect. <i>arXiv</i>	740
690	Jitang Li and Jinzheng Li. 2024. Memory, conscious-	<i>preprint arXiv:2403.03853</i> .	741
691	ness and large language model. <i>arXiv preprint</i>	Anand Mishra, Shashank Shekhar, Ajeet Kumar Singh,	742
692	<i>arXiv:2401.02509</i> .	and Anirban Chakraborty. 2019. Ocr-vqa: Visual	743
693	Junnan Li, Dongxu Li, Silvio Savarese, and Steven Hoi.	question answering by reading text in images. In	744
694	2023. Blip-2: Bootstrapping language-image pre-	<i>ICDAR</i> .	745
695	training with frozen image encoders and large lan-	Rui Pan, Xiang Liu, Shizhe Diao, Renjie Pi, Jipeng	746
696	guage models. <i>arXiv preprint arXiv:2301.12597</i> .	Zhang, Chi Han, and Tong Zhang. 2024. Lisa: Lay-	747
697	Chen Liang, Simiao Zuo, Qingru Zhang, Pengcheng	erwise importance sampling for memory-efficient	748
698	He, Weizhu Chen, and Tuo Zhao. 2023. Less is	large language model fine-tuning. <i>arXiv preprint</i>	749
699	more: Task-aware layer-wise distillation for language	<i>arXiv:2403.17919</i> .	750
700	model compression. In <i>International Conference on</i>	Alec Radford, Jong Wook Kim, Chris Hallacy, Aditya	751
701	<i>Machine Learning</i> , pages 20852–20867. PMLR.	Ramesh, Gabriel Goh, Sandhini Agarwal, Girish Sas-	752
702	Baohao Liao, Shaomu Tan, and Christof Monz. 2024.	try, Amanda Askell, Pamela Mishkin, Jack Clark,	753
703	Make pre-trained model reversible: From parameter	et al. 2021. Learning transferable visual models from	754
704	to memory efficient fine-tuning. <i>Advances in Neural</i>	natural language supervision. In <i>International confer-</i>	755
705	<i>Information Processing Systems</i> , 36.	<i>ence on machine learning</i> , pages 8748–8763. PMLR.	756
706	Tsung-Yi Lin, Michael Maire, Serge Belongie, James	Terri L Scott, Jeanne Gallée, and Evelina Fedorenko.	757
707	Hays, Pietro Perona, Deva Ramanan, Piotr Dollár,	2017. A new fun and robust version of an fmri local-	758
708	and C Lawrence Zitnick. 2014. Microsoft coco:	izer for the frontotemporal language system. <i>Cogni-</i>	759
709	Common objects in context. In <i>Computer Vision–</i>	<i>tive neuroscience</i> , 8(3):167–176.	760
710	<i>ECCV 2014: 13th European Conference, Zurich,</i>	Amanpreet Singh, Vivek Natarajan, Meet Shah,	761
711	<i>Switzerland, September 6-12, 2014, Proceedings,</i>	Yu Jiang, Xinlei Chen, Dhruv Batra, Devi Parikh,	762
712	<i>Part V 13</i> , pages 740–755. Springer.	and Marcus Rohrbach. 2019. Towards vqa models	763
713	Haotian Liu, Chunyuan Li, Qingyang Wu, and Yong Jae	that can read. In <i>Proceedings of the IEEE/CVF Con-</i>	764
714	Lee. 2023a. Visual instruction tuning. <i>arXiv preprint</i>	<i>ference on Computer Vision and Pattern Recognition</i>	765
715	<i>arXiv:2304.08485</i> .	(CVPR).	766
		Shuaiwen Leon Song, Bonnie Krufft, Minjia Zhang,	767
		Conglong Li, Shiyang Chen, Chengming Zhang,	768
		Masahiro Tanaka, Xiaoxia Wu, Jeff Rasley, Am-	769
		mar Ahmad Awan, et al. 2023. DeepSpeed4science	770

initiative: Enabling large-scale scientific discovery through sophisticated ai system technologies. *arXiv preprint arXiv:2310.04610*.

Mirac Suzgun, Nathan Scales, Nathanael Schärli, Sebastian Gehrmann, Yi Tay, Hyung Won Chung, Aakanksha Chowdhery, Quoc V Le, Ed H Chi, Denny Zhou, et al. 2022. Challenging big-bench tasks and whether chain-of-thought can solve them. *arXiv preprint arXiv:2210.09261*.

Hugo Touvron, Louis Martin, Kevin Stone, Peter Albert, Amjad Almahairi, Yasmine Babaei, Nikolay Bashlykov, Soumya Batra, Prajwal Bhargava, Shruti Bhosale, et al. 2023. Llama 2: Open foundation and fine-tuned chat models. *arXiv preprint arXiv:2307.09288*.

Maria Tsimpoukelli, Jacob L Menick, Serkan Cabi, SM Eslami, Oriol Vinyals, and Felix Hill. 2021. Multimodal few-shot learning with frozen language models. *Advances in Neural Information Processing Systems*, 34:200–212.

Guangxuan Xiao, Ji Lin, Mickael Seznec, Hao Wu, Julien Demouth, and Song Han. 2023. Smoothquant: Accurate and efficient post-training quantization for large language models. In *International Conference on Machine Learning*, pages 38087–38099. PMLR.

Licheng Yu, Patrick Poirson, Shan Yang, Alexander C Berg, and Tamara L Berg. 2016. Modeling context in referring expressions. In *Computer Vision—ECCV 2016: 14th European Conference, Amsterdam, The Netherlands, October 11–14, 2016, Proceedings, Part II 14*, pages 69–85. Springer.

Wenxuan Zhang, Paul Janson, Rahaf Aljundi, and Mohamed Elhoseiny. 2024a. Overcoming generic knowledge loss with selective parameter update. In *Proceedings of the IEEE/CVF Conference on Computer Vision and Pattern Recognition*, pages 24046–24056.

Yulin Zhang, Yanhua Li, and Junhan Liu. 2024b. Unified efficient fine-tuning techniques for open-source large language models.

Jun Zhao, Zhihao Zhang, Yide Ma, Qi Zhang, Tao Gui, Luhui Gao, and Xuanjing Huang. 2023. Unveiling a core linguistic region in large language models. *arXiv preprint arXiv:2310.14928*.

Deyao Zhu, Jun Chen, Xiaoqian Shen, Xiang Li, and Mohamed Elhoseiny. 2023. Minigpt-4: Enhancing vision-language understanding with advanced large language models. *arXiv preprint arXiv:2304.10592*.

A Details of Layer Importance Metrics

To demonstrate the effectiveness of our heuristically identified sparsely and uniformly distributed visual region, we conduct a comparative analysis against several other layer importance metrics (originally for layer pruning) by selecting 8 layers and

re-training Bunny-Llama-3-8B-V. Below are the details of how these metrics are calculated.

- **Block Influence (BI) Score (Men et al., 2024):** serves as an indicator of layer importance by measuring the transformation of hidden states. We utilize the Flickr30k dataset (Jia et al., 2015) to calculate the BI score for each layer within LVLMs. The BI score of i^{th} layers is calculated as following:

$$BI_i = 1 - \mathbb{E}_{X,t} \frac{X_{i,t}^T X_{i+1,t}}{\|X_i\|_2 \|X_{i+1}\|_2}$$

where X_i represents the hidden states of the i^{th} layer and $X_{i,t}$ denotes the hidden states of the t^{th} token at the i^{th} layer. By calculating the average cosine similarity of token states before and after passing through a layer, we measure the change magnitude across all tokens.

- **Multimodal BI Score:** As the above method treats visual image and text as a single modality, we propose a multimodal variant that separately calculates the hidden state transformations of visual tokens and textual tokens, and take its average as a multimodal BI score. The Multimodal BI score of i^{th} layers is calculated as follows.

$$BI'_i = 1 - \frac{1}{2} \left(\mathbb{E}_{X,t} \frac{X_{i,t}^T X_{i+1,t}}{\|X_i\|_2 \|X_{i+1}\|_2} + \mathbb{E}_{Y,l} \frac{Y_{i,l}^T Y_{i+1,l}}{\|Y_i\|_2 \|Y_{i+1}\|_2} \right)$$

$X_{i,t}$ and $Y_{i,l}$ respectively mean the hidden states of the t^{th} visual token and the l^{th} text token at the i^{th} layer. We calculate the cosine similarity of each modality tokens before and after passing through a layer, then average the results. This balances the token quantity across various modalities.

- **Parameter Change Ratio (Zhao et al., 2023):** We calculate the relative change ratio of the parameters in LVLM against its backbone LLM across each layer (by averaging all parameters within each layer). The parameter change ratio of i^{th} layers is calculated as follows:

$$R_i = \mathbb{E}_{\theta \in L_{i,j}} \left| \frac{\theta'_j - \theta_j}{\theta_j} \right|$$

where θ_j and θ'_j respectively mean the j^{th} parameter of layer L_i in LLM and LVLM.

- **Angular Distance (Gromov et al., 2024):** We calculate the Angular Distance of the parameters in LVLM against its backbone LLM across each layer (by averaging all parameters within each layer). The Angular Distance of i^{th} layers is calculated as follows:

$$D_i = \frac{1}{\pi} \arccos \left(\frac{\theta'_j \cdot \theta_j}{\|\theta'_j\| \|\theta_j\|} \right)$$

where θ_j and θ'_j respectively mean the j^{th} parameter of layer L_i in LLM and LVLM, $\|\cdot\|$ denotes the L^2 -norm and the factor of $\frac{1}{\pi}$ is a constant.

- **Image Attention Score:** We calculate image attention score to measure each layer’s affinity for image information. We utilize the DocVQA, OCRVQA, TDIUC, and RefCOCOg datasets, sampling 50 instances from each dataset to calculate the attention scores of the all image tokens for each layer within Bunny-Llama-3-8B-V. The heat map of image attention Score of every instances for each layers in Bunny-Llama-3-8B-V is showed in Figure 5. The image attention score of one instance in i^{th} layers A_i is calculated as follows:

$$A_i = \frac{\sum_{t=k}^{k+N_{\text{img}}-1} \sum_{h=1}^H \sum_{j=1}^T \text{Attn}[i][h, j, t]}{N_{\text{img}}H}$$

where H represents the number of attention heads per layer and T denotes the total number of tokens at the i^{th} layer. N_{img} is the number of image tokens of the instance. The index range for the image tokens is from k to $k + N_{\text{img}} - 1$. While $\text{Attn}[h, j, t]$ means the attention score of the h^{th} attention head for the j^{th} token to the t^{th} token.

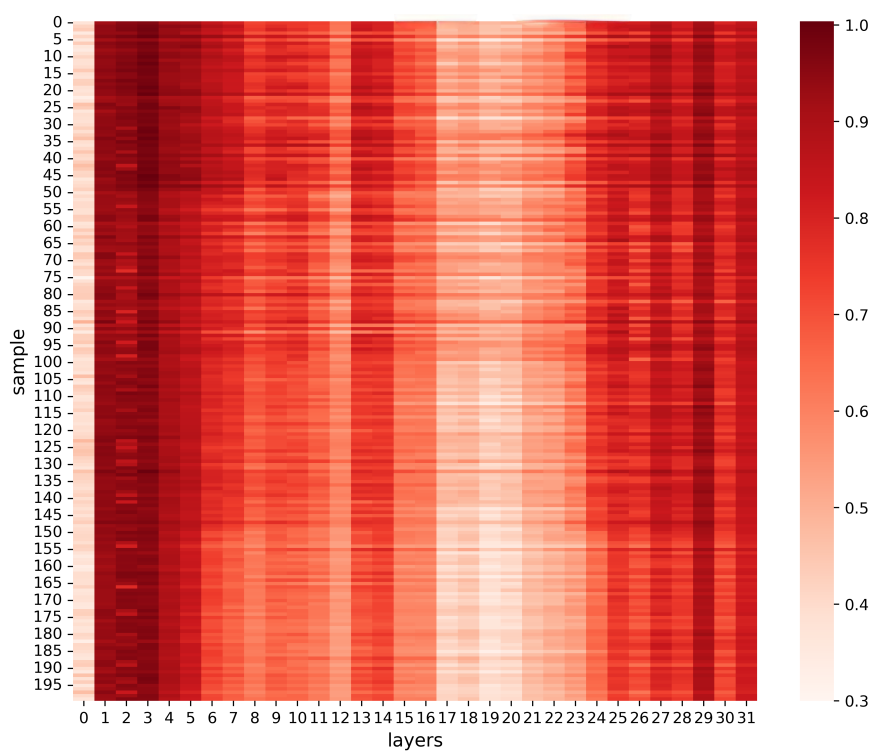


Figure 5: Visualization of Image Attention Scores for every instances across all layers